Microgel encapsulated nanoparticles for glucose-responsive insulin delivery

Microgel encapsulated nanoparticles for glucose-responsive insulin delivery

Lisa R. Volpatti, Amanda L. Facklam, Abel B. Cortinas, Yen-Chun Lu, Morgan A. Matranga, Corina MacIsaac, Michael C. Hill, Robert Langer, and Daniel G. Anderson*

L. R. Volpatti, A. B. Cortinas, M. A. Matranga, M. C. Hill, R. Langer, D. G. Anderson
Department of Chemical Engineering
Massachusetts Institute of Technology
Cambridge, MA 02139, USA

L. R. Volpatti, A. L. Facklam, A. B. Cortinas, Y.-C. Lu, C. MacIsaac, R. Langer, D. G. Anderson
David H. Koch Institute for Integrative Cancer Research
Massachusetts Institute of Technology
Cambridge, MA 02139, USA

A. L. Facklam, R. Langer
Department of Biological Engineering
Massachusetts Institute of Technology
Cambridge, MA 02139, USA

Y.-C. Lu, R. Langer, D. G. Anderson
Department of Anesthesiology
Boston Children's Hospital
Boston, MA 02115, USA

C. MacIsaac, R. Langer, D. G. Anderson
Harvard–Massachusetts Institute of Technology Division of Health Sciences and Technology
Institute for Medical Engineering and Science
Massachusetts Institute of Technology
Cambridge, MA 02139, USA

E-mail: dgander@mit.edu

Abstract: An insulin delivery system that self-regulates blood glucose levels has the potential to limit hypoglycemic events and improve glycemic control. Glucose-responsive insulin delivery systems have been developed by coupling glucose oxidase with a stimuli-responsive biomaterial. However, the challenge of achieving desirable release kinetics (i.e., insulin release within minutes after glucose elevation and duration of release on the order of weeks) still remains. Here, we develop a glucose-responsive delivery system using encapsulated glucose-responsive, acetalated-dextran nanoparticles in porous alginate microgels. The nanoparticles respond rapidly to changes in glucose concentrations while the microgels provide them with protection and stability, allowing glucose-responsive insulin release for at least 28 days. This system reduces blood sugar in a diabetic mouse model at a rate similar to naked insulin and responds to a glucose challenge 3 days after administration similarly to a healthy animal. With 2 doses of microgels containing 60 IU/kg insulin each, we are able to achieve extended glycemic control in diabetic mice for 22 days.

1. Introduction

Diabetes mellitus is a disease characterized by poor glycemic control as a result of deficient insulin production (Type 1) or signaling (Type 2). Type 1 and advanced Type 2 diabetic patients are dependent on exogenous insulin to combat hyperglycemia [1]. Despite many advancements in treatment since the discovery of insulin in 1921, diabetes continues to grow in prevalence worldwide and remains a leading cause of death in the United States [2, 3]. As a result of chronic hyperglycemia, diabetic patients are at a higher risk of blindness, cardiovascular disease, and kidney failure [4-6]. The standard of care for many insulin-dependent diabetic patients involves consistent self-monitoring of blood glucose levels from finger pricks in conjunction with multiple daily subcutaneous injections of insulin in attempt to achieve normoglycemia. However, self-administration fails to tightly regulate blood glucose levels and increases the risk hypoglycemia which can lead to seizures, unconsciousness, and death [7, 8]. A self-regulated delivery system in which glucose sensing is directly coupled to insulin therapy would result in fewer hypoglycemic events and better long-term glycemic control.

One such delivery system comes in the form of an insulin pump that combines continuous glucose sensing with insulin infusions [9]. However, there are still many challenges associated with current devices. Most continuous glucose monitors require recalibration with blood glucose levels from a finger prick and have a limited lifetime [10-12]. Insulin pump technology also requires patients to be educated on its use for proper insertion and removal, decision making, and response to alarms [13]. Therefore, although these systems may be considered “closed-loop,” they still place a burden of responsibility on the patient.

In attempt to reduce this patient burden, chemically glucose-responsive insulin delivery systems have been developed. These systems can largely be classified as nanoparticles, hydrogels, microgels, or membranes that encapsulate insulin and may shrink, swell, or degrade in response to glucose to release the therapeutic protein on demand [14, 15]. The most commonly employed glucose sensors are phenylboronic acid and glucose oxidase (GOx). Phenylboronic acid is a small molecule that becomes ionized upon binding to diols. Therefore, polymer networks containing these moieties as pendant groups swell in response to high levels of sugar as a result of the change in osmotic pressure [16-19]. Phenylboronic acids, as well as glucose binding proteins, are also used to create covalent crosslinks that are displaced upon competitive binding when the surrounding glucose concentration is high [20-22].

For enhanced specificity to glucose, some formulations employ GOx – an enzyme that converts glucose to gluconolactone, which is readily hydrolyzed into gluconic acid, and produces hydrogen peroxide as a byproduct. Insulin release rates can therefore be enhanced when glucose levels are high by encapsulating both GOx and insulin in a pH-responsive or peroxide-sensitive polymeric delivery vehicle [23-25]. pH-responsive systems containing GOx often employ the second enzyme catalase to disproportionate the hydrogen peroxide and regenerate the oxygen needed for the catalytic conversion of glucose [26]. The combination of these two enzymes can provide sustained glucose sensing in situ [26].

Ideally, a glucose-responsive insulin delivery system would provide long-term glycemic control with reduced dosing frequency, respond rapidly and autonomously to changes in blood glucose levels, and limit the occurrence of hypoglycemic events. While there have been reports of insulin

release in response to glucose in vitro, no chemically actuated drug delivery system has yet translated [27, 28].

To overcome challenges in obtaining desired release kinetics and achieving both rapid and long-term glycemic control, here we encapsulate glucose-responsive nanoparticles (NPs) into porous microgels. Microgels are readily formed from crosslinking alginate, an inherently biocompatible and naturally available material, with divalent cations, including calcium and barium [29, 30]. NPs are synthesized from the pH-sensitive polymer acetalated-dextran (Ac-dex) [31, 32] and encapsulate insulin, GOx, and catalase. A co-formulation of two populations of nanoparticles, one with rapid release kinetics and the other with more extended release [33], are preconcentrated into alginate microgels which serve as a subcutaneous depot of glucose-responsive insulin in vivo. Thus, we are able to combine the large surface area of nanoparticles with the stable porous network of microgels to create a system that 1) responds to a glucose challenge with a corresponding increase in serum insulin levels within 30 min and 2) achieves prolonged normoglycemia for over 3 weeks with 2 doses in diabetic mice.

2. Materials and Methods

All chemicals were obtained from Sigma-Aldrich (St. Louis, MO) and cell culture reagents from Life Technologies (Carlsbad, CA) unless otherwise noted. Recombinant human insulin (Gibco™) was purchased from ThermoFisher Scientific (Waltham, MA). AlphaLISA SureFire ULTRA kits were purchased from Perkin-Elmer (Waltham, MA) to quantify AKT phosphorylation, and an insulin ELISA kit was purchased from ALPCO (Salem, NH) to measure serum insulin.

2.1. Nanoparticle synthesis

Acetalated-dextran nanoparticles were prepared with a double-emulsion, solvent evaporation technique. Briefly, 50 mg insulin was dissolved in 0.5 mL carbonate buffer (pH 9.5) with or without 11 mg GOx (128.2 units/mg) and 1.5 mg catalase (≥20,000 units/mg) and added to 6 mL DCM containing 240 mg Ac-Dex. This two-phase mixture was sonicated for 90 s (Q-500, QSonica, 65% amplitude) with 1 s pulse and immediately added to 25 mL 3% poly(vinyl alcohol) (PVA) in PBS solution. After a second round of sonication, the emulsion was added to 150 mL of a 0.3% PVA solution. The mixture was stirred at room temperature for 2 h, centrifuged (15 min, 8000 rcf; Avanti JXN-26, Beckman Coulter) and washed twice with basic water (pH 8). The resultant nanoparticles were lyophilized and stored at -20 °C until use.

2.2. Microgel synthesis

Alginate microgels were fabricated with a custom-designed, electro-spray system comprised of a vertically mounted syringe pump, a voltage generator, and a grounded metal collecting dish containing $CaCl_2$ (50 mM) or $BaCl_2$ (20 mM) gelling solution. Microgels were formed from a 1.4% solution of PRONOVA SLG20 (NovaMatrix, Sandvika, Norway) dissolved in a 20 mg/mL suspension of nanoparticles in 0.9% saline. A 25 G 1.5 in blunt needle with a voltage of 7.5 kV and a flow rate of 180 µl/min were used to generate microgels with an average diameter of 415 µm. After crosslinking, the microgels were washed with saline containing 2 mM $CaCl_2$ and stored at 4 °C until use.

2.3. In vitro insulin release

Acid-mediated insulin release from free nanoparticles was determined by incubating 5 mg/mL nanoparticles without enzymes in PBS (pH 7.4) or acetate buffer (pH 5) at 37 °C with agitation. At indicated time points, aliquots were withdrawn and centrifuged. The supernatants were removed and insulin content was analyzed with a Coomassie Plus protein assay (Pierce) according to the manufacturer's protocol. To determine insulin release from microgels, 100 µL of microgels and 400 µL buffer (PBS or acetate with 2 mM $CaCl_2$) were incubated at 37 °C with agitation. At indicated time points, 100 µL of buffer was exchanged and analyzed with a Coomassie Plus protein assay for total protein content. For glucose-mediated release, 120 µL of suspended microgels with enzymes and 170 µL of buffer (PBS, 100 mg/dL glucose in PBS, or 400 mg/dL glucose in PBS) were added to 200 µL centrifuge tubes. The tubes were incubated in a 37 °C shaker, and the buffer was exchanged every two hours. The total protein content of these samples was determined with a Coomassie Plus protein assay.

2.4. Bright field and fluorescence microscopy

Microgels were imaged immediately prior to and following incubation (400 mg/dL glucose, 37 °C, 24 h) using an EVOS Xl bright field microscope (Advanced Microscopy Group). ImageJ software was used to measure the diameter of > 2500 microgels from bright field images. At predetermined time points after incubation in PBS containing 2 mM $CaCl_2$ and 400 mg/dL glucose, aliquots of microgels loaded with insulin conjugated with fluorescein isothiocyanate (FITC) were rinsed with PBS containing 2 mM $CaCl_2$ and imaged with an EVOS Xl fluorescent microscope (Advanced Microscopy Group). ImageJ software was used to quantify the decrease in fluorescence intensity.

2.5. Confocal microscopy

Microgels were fabricated with nanoparticles containing FITC-insulin and glucose oxidase and catalase conjugated with Alexa Fluor 647. After washing the microgels with saline with 2 mM $CaCl_2$ several times, they were transferred to a black, glass bottom plate and imaged with a confocal microscope (Olympus FV1200). ImageJ software was used to recolor the images and create a maximum intensity projection by stacking 45 images taken at ~ 10 µm increments.

2.6. Circular dichrosim

Secondary structure motifs were elucidated using high-performance circular dichroism (CD). Naked recombinant human insulin and nanoparticle-encapsulated microgels were incubated in PBS at 37 °C over a period of 9 days. At indicated time points, aliquots of naked insulin and microgels were withdrawn. Insulin was released from the microgels following the addition of acid and both naked and released insulin (200 µg/mL) were analyzed with a high-performance CD spectrometer (J-1500, JASCO Inc.) over a wavelength range of 200–250 nm using a 0.1 cm pathlength cell.

2.7. In vitro insulin activity

The in vitro activity of released insulin was determined with a cellular AKT assay. To prepare for the AKT assay, C2C12 cells (American Type Culture Collection) were cultured in Dulbecco's modified Eagle medium (DMEM) containing L-glutamine, 4.5 g/L D-glucose, and 110 mg/L sodium pyruvate supplemented with 10% fetal bovine serum and 1% penicillin–streptomycin. Cells were seeded and incubated in 96-well plates at a density of 5,000 cells per well. After 24 h, the cells were washed twice with serum-free DMEM and incubated for 4 h. The media was then removed, and the cells were stimulated with insulin samples or controls for 30 min. The cells were then washed twice with cold Tris-buffered saline and lysed with cold Lysis Buffer (Perkin-Elmer) for 10

min. Concentrations of pAKT 1/2/3 (Ser473) and total AKT 1 in the cell lysates were determined with AlphaLISA SureFire ULTRA kits (Perkin-Elmer) according to the manufacturer's instructions. Data were analyzed using GraphPad Prism 6.0 and fit to four parameter dose-response curves to determine the EC50 of each insulin sample.

2.8. In vivo imaging studies

All animal protocols were approved by the MIT Committee on Animal Care, and animals were cared for under supervision of MIT's Division of Comparative Medicine. For in vivo imaging, 8-week-old male SKH1E mice (hairless, immunocompetent) were fed an alfalfa-free diet (AIN-76A, Bio-Serv) for 1 week leading up to the study to limit background fluorescence. Mice were anesthetized using inhaled isoflurane and imaged with an IVIS Spectrum in vivo imaging system with a heated chamber containing inhaled isoflurane. Alginate microgels were prepared with nanoparticles containing dextran (10 kDa) conjugated with AlexaFluor680. Mice were injected subcutaneously on the lateral flank with microgels or nanoparticles at a dose equivalent to 60 IU/kg insulin and imaged at several time points using filter sets of 640/760, medium binning, an F-stop of 1, and an exposure time of 0.5 s. Living Image software was used to analyzed the fluorescence efficiency and total flux of the images.

2.9. In vivo blood glucose studies

The safety and efficacy of nanoparticle-encapsulated microgels were evaluated using healthy and diabetic C57BL/6 mice (Jackson Labs). To induce diabetes, 8-week-old male mice were injected with a single dose of 150 mg/kg streptozotocin. Blood glucose levels were monitored for the following week, and only mice with blood glucose levels consistently over 400 mg/dL were considered diabetic. Groups of at least 4 mice were fasted for 10 h and subcutaneously injected with microgels, nanoparticles, or naked insulin. A ~ 1 µL drop of blood from the tail vain was used to monitor blood glucose levels every 30 min with Clarity BG1000 Blood Glucose Meters. For long term studies, mice were fasted 10 h prior to measuring their blood glucose. Glucose tolerance tests were performed by administering 1.5 – 3 g/kg glucose in saline solution to the mice intraperitoneally.

2.10. In vivo serum insulin studies

To measure serum insulin concentration, blood was collected by terminal cardiac punctures into serum gel microtubes (BD SST™ Microtainer). After centrifugation (5 min, 7000 rcf), serum was collected and analyzed immediately using a human insulin enzyme-linked immunosorbent assay kit (ALPCO) according to the manufacturer's instructions.

2.11. Statistical analysis

Data are expressed as mean ± standard deviation unless otherwise indicated, and N = 4 – 6 randomly assigned mice per time point and per group. Data were analyzed for statistical significance by unpaired, two-tailed Student's t-tests or by one-way ANOVA with Bonferroni multiple comparison correction where indicated.

3. Results

3.1. Acetal-derivatized dextran nanoparticles are encapsulated inside alginate microgels.

To create a delivery system that rapidly responds to elevated glucose levels and also extends glucose-responsive insulin release to timescales on the order of weeks, we encapsulate pH-sensitive NPs containing insulin, GOx, and catalase into porous alginate microgels (Fig. 1a). Due to the opacity of the NPs, the NP-encapsulated microgels ("microgels") do not allow light to pass through and appear dark in bright field microscopy images (Fig. 1b). When glucose levels are high, GOx converts glucose into gluconic acid, thus lowering the pH of the environment inside the microgel. NPs are synthesized from an acetal-derivatized dextran (Ac-dex) with varying degrees of modification (Fig. S1). Under acidic conditions, the acetal bonds are rapidly cleaved, solubilizing the dextran, releasing the encapsulated cargo, and leaving the translucent alginate microgel shell (Fig. 1c).

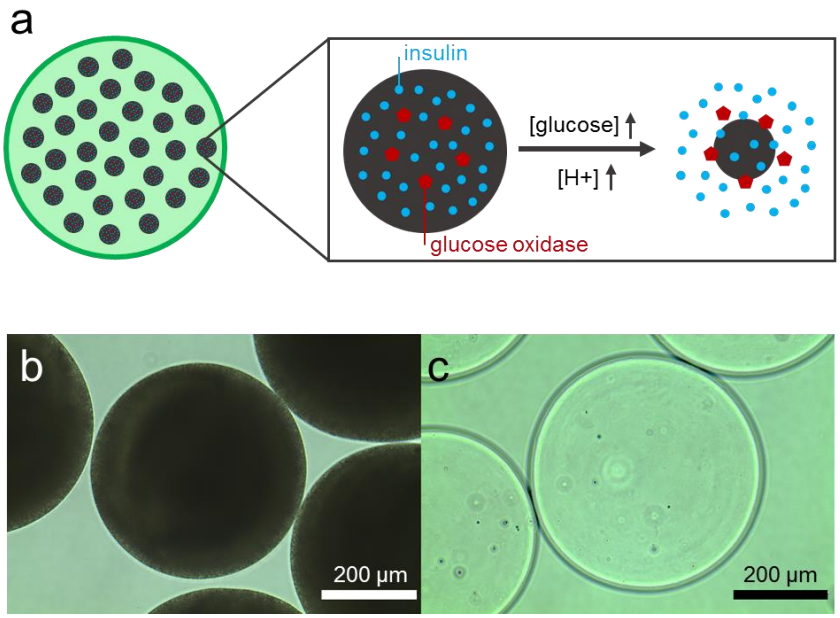

Figure 1. Ac-dextran nanoparticles can be encapsulated and degraded in alginate microgels. a) Schematic of encapsulation and glucose-responsive insulin release from acid-degradable Ac-dex NPs. b) Bright field microscopy image of NP-encapsulated alginate microgels. c) Alginate microgels in (b) upon exposure to 400 mg/dL glucose for 24 h, showing the degradation of the NPs.

By analyzing the NMR of the degradation products, we can determine the percent modification of each Ac-dex polymer (Fig. S2). Reacting dextran for 10 min yields a polymer in which 55% of residues have a cyclic acetal modification, while reacting for 20 min yields a polymer with 71% cyclic modifications. Since the percentage of cyclic modifications correlates with polymer stability, these different polymers show different kinetics of degradation [33]. A double emulsion method is used to synthesize NPs that encapsulate insulin, GOx, and catalase. The NPs from the 10 min polymer and the 20 min polymer are similar in size, with an average diameter of 275 nm (Fig. S3). The average insulin loading capacity of these NPs is 6.5% insulin and 0.68% GOx, with loading

efficiencies of 39% and 19%, respectively (Fig. S4). A mixture of the 10 min and 20 min NPs provides both rapid and extended glucose-responsive insulin release [33].

To encapsulate the NPs, we add the mixture of 10 min and 20 min NPs to an alginate solution and use a custom-designed electro-spray system to create microdroplets, which are rapidly crosslinked by divalent cations in a gelation bath to form microgels (see methods). Since Ba^{2+}-crosslinked alginate microgels and Ca^{2+}-crosslinked alginate microgels are known to have differing mechanical properties and porosity [30], both cations were tested in this study to optimize microgel stability and insulin release kinetics. When Ba^{2+} is used as a crosslinker, there is an additional barrier to diffusion leading to a delay in acid-mediated insulin release in comparison to free NPs (Fig. 2a). However, when alginate is crosslinked with Ca^{2+}, microgels exhibit insulin release kinetics similar to those of free NPs, with over 80% of insulin released in the first hour (Fig. 2a). Both cations yield microgels that are stable under PBS at pH 7.4 with physiological concentrations of Ca^{2+} (2 mM), resulting in less than 10% of insulin being released over 11 h (Fig. 2a). To further probe acid-mediated release kinetics from Ca^{2+}-crosslinked microgels, we analyzed the release profiles when microgels are subjected to fluid flow. Upon incubation in a perifusion chamber with a flow rate of 10 µL/min acetate buffer (pH 4.7), microgels exhibit comparable insulin release kinetics to those without any fluid flow (Fig. S5). However, there is a slight delay in the onset of release, possibly due to the low flow rate and limited mixing occurring in the chamber.

The diameters of a sample (> 2500) of Ca^{2+}-crosslinked microgels approximate a Gaussian distribution with a mean of 411 µm and a standard deviation of 86 µm (Fig. 2b). To determine the distribution of NPs within the microgels, NPs were synthesized containing fluorescein isothiocyante (FITC)-labeled insulin and AlexaFluor 647 (AF647)-labeled GOx. We then encapsulated these NPs in microgels and imaged them using confocal microscopy. A maximum intensity projection shows that the proteins are co-localized and the NPs are evenly distributed throughout the microgels (Fig. 2c). Additional confocal images of a single z-plane of the microgels show a dark core due to the low transmittance of light through the densely packed NPs (Fig. S6).

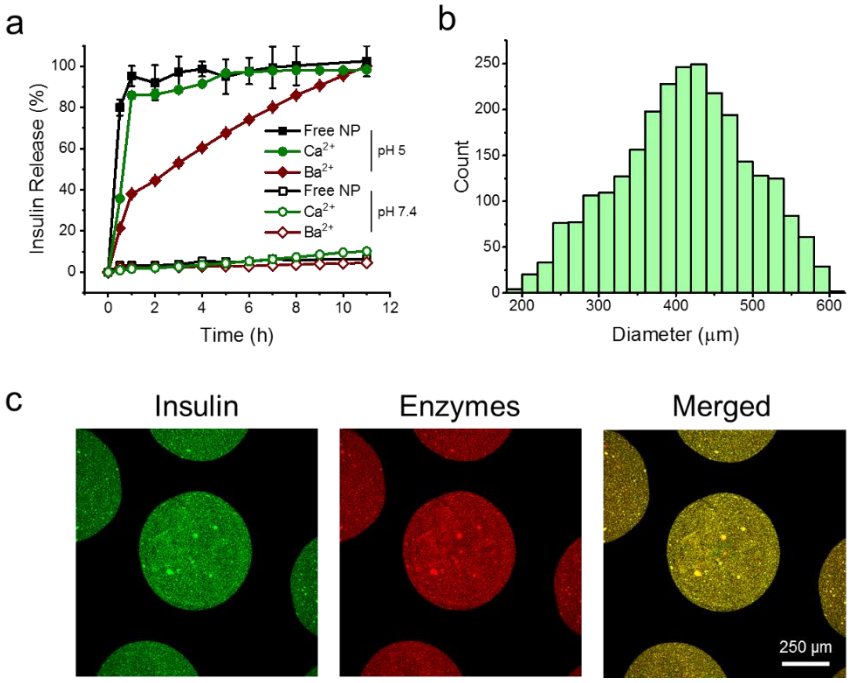

Figure 2. Insulin release can be tuned from uniform NP-encapsulated microgels a) Insulin release from free NPs, NPs encapsulated in Ca^{2+}-crosslinked microgels, or NPs encapsulated in Ba^{2+}-crosslinked microgels incubated in either acetate buffer (pH 5) or phosphate buffered saline (PBS, pH 7.4) at 37 °C with agitation. b) Histogram of microgel diameter for over 2500 microgels, with an average diameter of 411 μm. c) Maximum intensity projection of confocal microscopy images of microgels containing NPs encapsulated with FITC-insulin and AF647-glucose oxidase.

3.2. Microgels achieve glucose-responsive insulin release in vitro.

To probe the kinetics of insulin release, FITC-insulin NPs were loaded into microgels, and fluorescent images were taken at various time points following incubation in PBS with 400 mg/dL glucose (Fig. 3a). Image quantification shows that the largest decrease in fluorescence occurs after 2 h of incubation (Fig. 3b). Microgels were then incubated in PBS alone, PBS containing 100 mg/dL glucose (normal glucose conditions), or PBS containing 400 mg/dL glucose (elevated glucose conditions) with complete buffer exchange every 2 h. Under these conditions, the largest increase in protein release in the 400 mg/dL glucose solution occurs after 4 h of incubation (Fig. 3c). Less than half of the total protein is released over a 10 h period under physiological concentrations of glucose, and minimal protein is released in PBS alone (Fig. 3c). The glucose-mediated protein release profile from microgels is similar to that from free NPs when directly compared under analogous release conditions (e.g., concentrations, frequency of buffer exchange, Fig. S7).

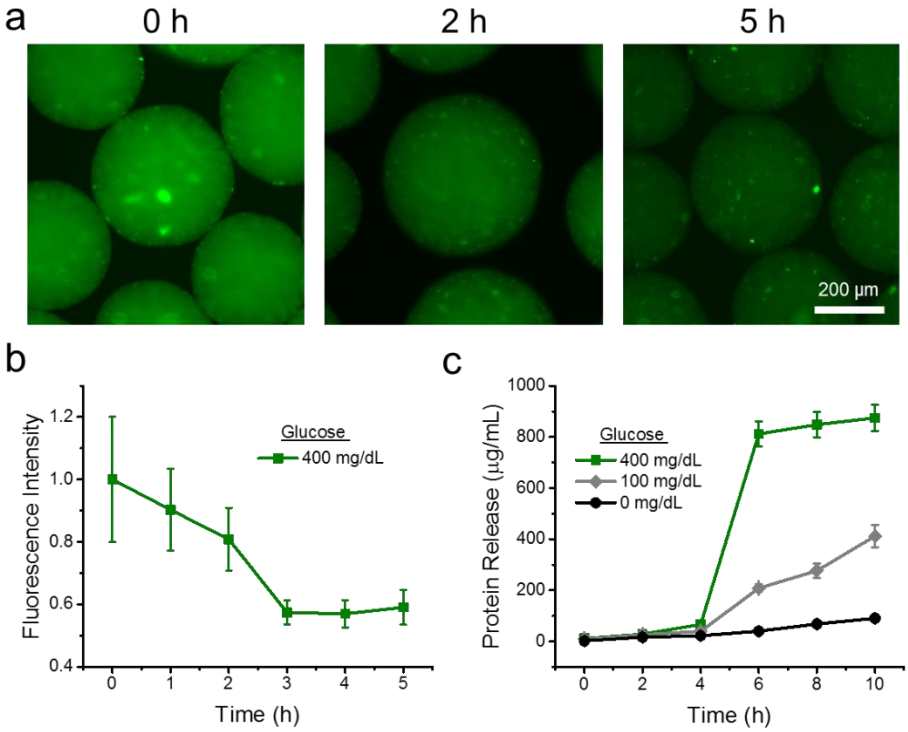

Figure 3. Insulin is released from NP-encapsulated microgels in response to elevated glucose concentrations. a) Fluorescence microscopy images of microgels loaded with FITC-insulin nanoparticles. At predetermined time points after incubation in PBS containing 400 mg/dL glucose, aliquots of microgels were rinsed with PBS and imaged. b) Quantification of fluorescence intensity of images from (a) over time. c) Total protein release from microgels incubated in PBS containing 400, 100, or 0 mg/dL glucose. Every 2 h, insulin content in the supernatant was analyzed and the buffer was replaced.

3.3. Encapsulated insulin retains structure and activity upon incubation.

Next, we analyzed the structure and activity of the released insulin in vitro. Naked insulin and microgels were incubated at 37 °C with agitation for 0, 3, or 9 days. At these time points, insulin was released from the microgels via acid-mediated Ac-dex degradation and analyzed in comparison to naked insulin. Circular dichroism (CD) was performed to characterize the secondary structure of insulin. As an α-helical protein, insulin exhibits a CD spectrum with negative bands at 222 nm and 208 nm [34, 35]. Prior to incubation, the spectra of both naked insulin and released insulin have these characteristic bands (Fig. 4a,b). However, after 3 days of incubation, the spectrum of naked insulin begins to lose the band at 222 nm, suggesting that it is denaturing in solution. By Day 9, this negative band is completely absent (Fig. 4a), consistent with reports of guanidine hydrochloride-induced denaturation of insulin [36]. The released insulin, on the other hand, which has been stabilized by the microgels during incubation retains its characteristic bands and its α-helical structure throughout the duration of the experiment (Fig. 4b).

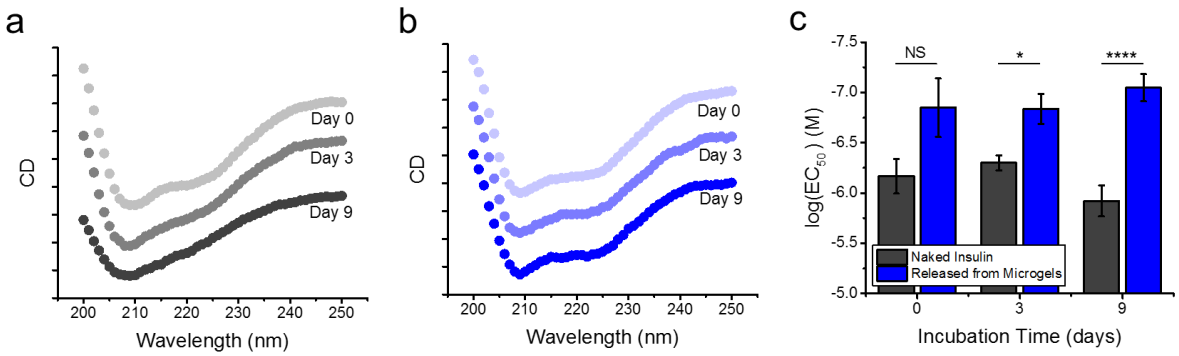

Figure 4. Insulin in microgels remains stable and active after 9 days of incubation. a) Circular dichroism spectra of insulin incubated in PBS at 37 °C with agitation for 0, 3, and 9 days, showing the loss of the negative band at 222 nm. b) Circular dichroism of insulin that has been released from microgels incubated in PBS at 37 °C with agitation for 0, 3, and 9 days, showing the retention of its secondary structure. c) EC_{50} determined by AKT phosphorylation of C2C12 cells exposed to naked insulin or insulin released from microgels after 0, 3, or 9 days of incubation. Data represent mean ± standard error of the mean. Statistical significance was evaluated by a two-tailed, unpaired t-test, and significance is indicated by *$p < 0.05$, ****$p < 0.0001$; NS: $p > 0.05$.

To determine if the retention of its secondary structure results in enhanced insulin activity, we performed a cell-based insulin receptor assay (see methods). By quantifying the extent of AKT phosphorylation resulting from the dose-dependent binding of insulin to its receptor, we can calculate an EC_{50} of the protein. When both naked insulin and microgels are incubated for 3 or 9 days, insulin newly released from the microgels is significantly more potent than the partially denatured naked insulin (Fig. 4c). These results support the hypothesis that microgels stabilize the insulin and protect it from denaturation for over a week in vitro (Fig. 4c), suggesting that they may have potential to act as long-term depots of insulin in vivo. Furthermore, these results suggest that processing, encapsulating, and releasing insulin do not adversely affect its structure or activity.

3.4. Microgels create depot of nanoparticles in vivo.

We next tested the ability of the microgels to remain at the site of injection and provide sustained release of insulin. We encapsulated AlexaFluor 680 (AF680)-labeled dextran into NPs and tracked the fluorescence of microgels or free NPs (N = 4) over time (Fig. 5a, S8). The control mouse received an injection of either empty microgels or empty NPs and was used to normalize the fluorescence values in each group. The initial fluorescence of the microgels is significantly lower than that of the free NPs, possibly due to the increased proximity of NPs and shielding of the fluorophore. Both microgels and NPs exhibit peak fluorescence one week post-administration as the Ac-dex degrades and exposes the AF680-dextran (Fig. 5b). Both groups subsequently experience a decrease in fluorescence when the AF680-dextran diffuses away or is cleared from the site of injection. After 21 and 28 days post-administration, the fluorescence of the NPs encapsulated in microgels is significantly higher than that of the free NPs (Fig. 5b).

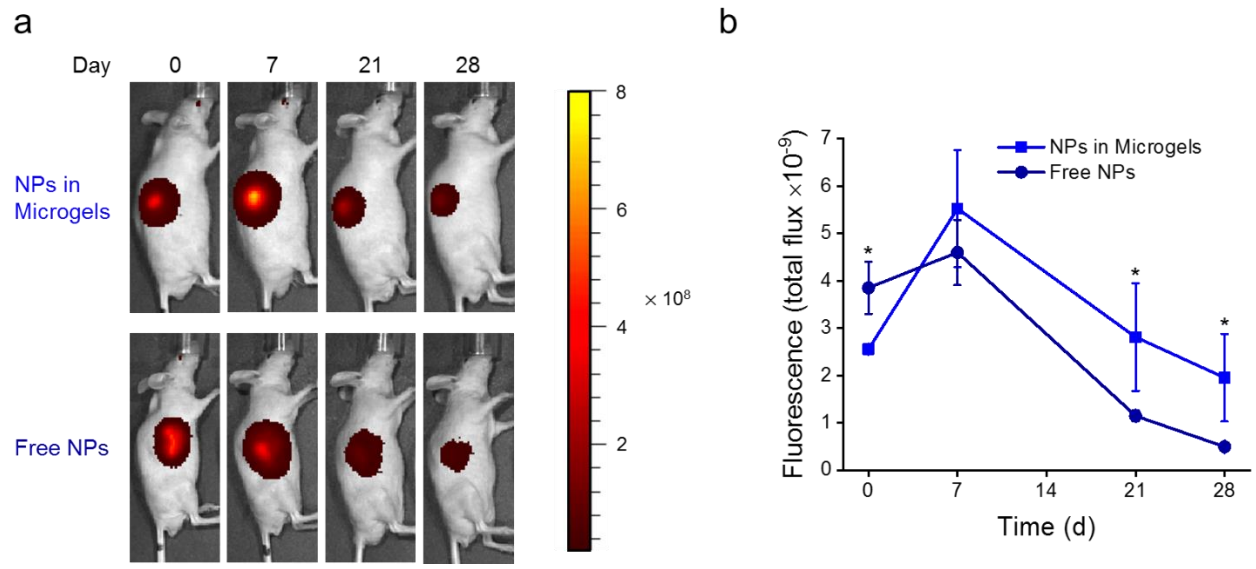

Figure 5. Microgels remain at the site of injection in healthy mice longer than free NPs. a) Representative in vivo fluorescent images of NP-encapsulated microgels or free NPs containing AF680-dextran (10 kDa) subcutaneously injected in mice at a dose of 35 mg NP/kg. b) Quantification of total flux of fluorescence in (a). Data represent mean ± standard deviation, normalized to background fluorescence of a control mouse. Statistical significance was evaluated by a two-tailed, unpaired t-test, and significance is indicated by *$p < 0.05$.

3.5. Hypoglycemia is reduced in healthy mice.

To determine whether the microgels offer enhanced protection from hypoglycemia in vivo, we monitored the blood glucose (BG) levels of fasted, healthy C57BL/6 mice following subcutaneous administration of microgels, naked insulin, or an empty microgel control. Mice receiving microgels at an insulin dose of 60 IU/kg remained normoglycemic (70 mg/dL < BG < 200 mg/dL) for the 8.5 h period, suggesting there is minimal leakage of insulin at this dose under normal glucose conditions (Fig. 6a). Conversely, the 3 IU/kg dose of naked insulin causes the mice to experience hypoglycemia within the first hour with BG levels below 70 mg/dL. This hypoglycemic effect is quantified by calculating the area above the curve (AAC) and under the average starting BG for the first 2.5 h, capturing the initial reduction in BG levels resulting from insulin administration. Using this metric, microgels at doses of 30 or 60 IU/kg show significantly reduced hypoglycemic effect compared to 3 IU/kg naked insulin, while doses of 115 and 225 IU/kg have comparable hypoglycemic effects (Fig. 6b, S9). The mice were monitored over the following 2 weeks with average fasted BG levels remaining in the normoglycemic range (Fig. 6c).

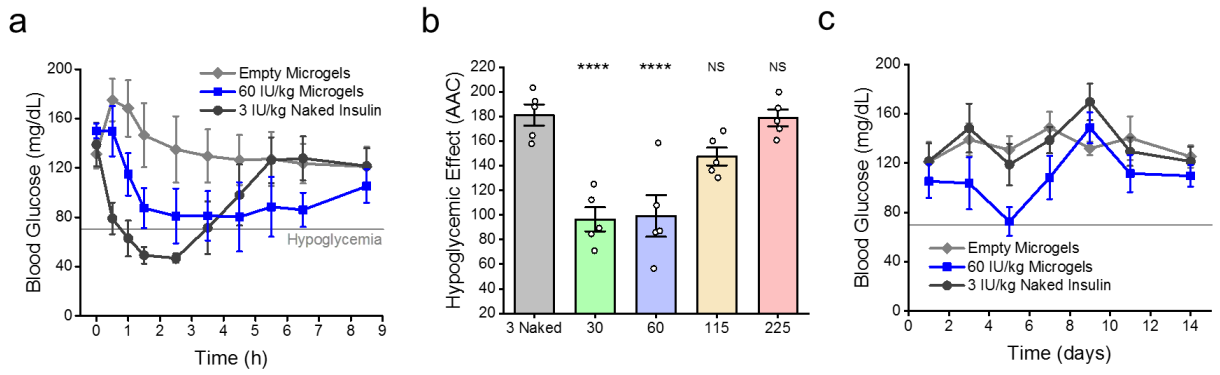

Figure 6. Microgels reduce the hypoglycemic effect of insulin in healthy mice. a) Blood glucose (BG) levels of healthy mice after administration of empty microgels, nanoparticle-encapsulated microgels at an insulin dose of 60 IU/kg, or naked insulin at a dose of 3 IU/kg. b) Quantification of treatments in (a) in addition to doses of 30, 115, and 225 IU/kg using the area above the curve (AAC) and below the average starting BG for the first 2.5 h to represent the hypoglycemic effect. Statistical significance was determined by one-way ANOVA with Bonferroni multiple comparison correction (****$p < 0.001$, NS: $p > 0.05$ in comparison to naked insulin group). c) Fasted blood glucose levels of mice in (a) over two weeks. Data represent mean ± standard deviation (a,c) or standard error of the mean (b).

3.6. Blood glucose is regulated in diabetic mice with glucose-responsive insulin release.

We next determined microgel efficacy in a streptozotocin (STZ)-induced type 1 diabetic mouse model. Fasted mice were subcutaneously injected with microgels, naked insulin, or an empty microgel control. The microgels reduced BG levels at virtually the same rate as naked insulin over the first hour (Fig. 7a), suggesting they can serve as a fast-acting system. To test the ability of the microgels to combat an increase in blood sugar, mice were intraperitoneally administered glucose tolerance tests (GTTs; 1.5 g/kg) every 2 h after the first hour. While the group receiving naked insulin reverted back to hyperglycemic after the first GTT, the group with microgels maintained tight glycemic control for the duration of the study following 4 GTTs (Fig. 7a).

To provide more direct evidence of glucose-responsive insulin release in vivo, we quantified the concentration of human insulin in diabetic mouse serum samples over time for mice receiving microgels with or without GOx and catalase. The pharmacokinetic profile of the group receiving enzymes exhibits a peak in insulin release following administration with an additional spike directly after a GTT (3 g/kg, Fig. 7b). The group without enzymes also shows a peak in insulin release after the first hour, indicative of nonspecific burst release; however, this peak is significantly reduced in comparison to the group receiving enzymes. Furthermore, there is no increase in insulin release following the GTT, suggesting that enzymes are needed for glucose-responsiveness.

To probe the efficacy of the microgels as a sustained insulin depot with prolonged glycemic control, we administered a GTT (3 g/kg) to fasted mice 3 days following microgel dosing. The BG response of the treated mice overlays that of naïve mice while mice receiving empty microgels fail to achieve normoglycemia (Fig. 7c). These results are quantified using the area under the curve (AUC), which shows there is no significant difference between treated and naïve mice, and both groups have significantly reduced BGs compared to those from the empty microgel group (Fig. 7d).

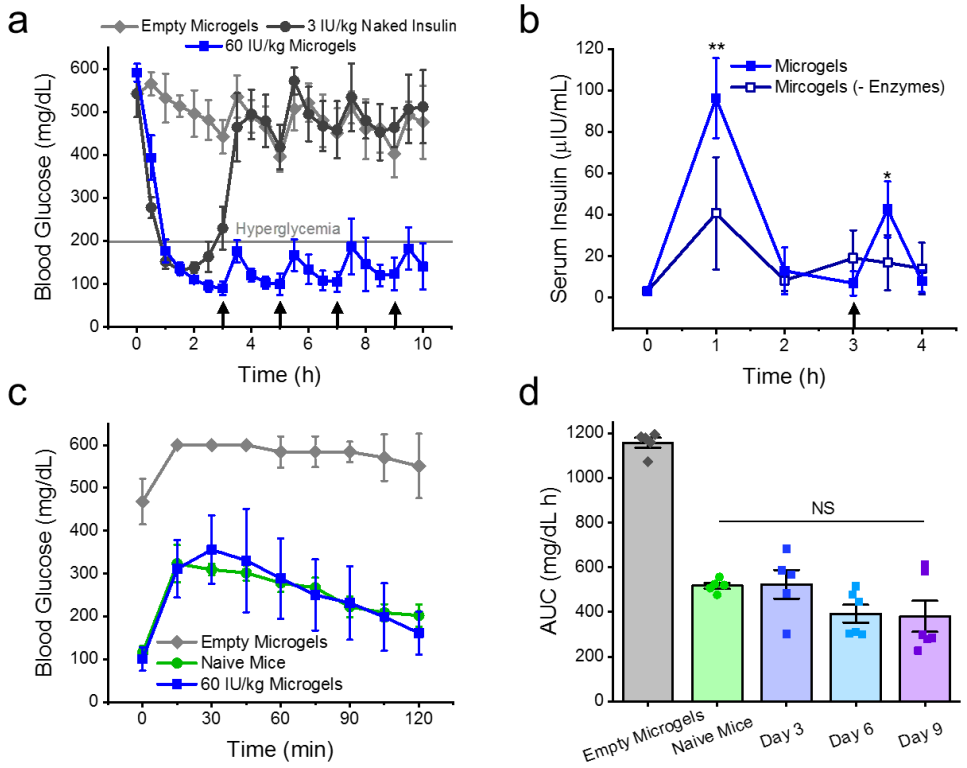

Figure 7. Microgels exhibit short-term glycemic control and glucose-responsive insulin release in diabetic mice. a) Blood glucose levels of STZ-induced type 1 diabetic mice following subcutaneous administration of empty microgels, naked insulin, or NP-encapsulated microgels. Arrows represent intraperitoneal glucose tolerance tests (GTTs, 1.5 g/kg). b) Concentration of human insulin in diabetic mouse serum following the injection of microgels (with or without enzymes) with a GTT (3 g/kg) at 3 h. Statistical significance was evaluated by a two-tailed, unpaired t-test, and significance is indicated by *$p < 0.05$, **$p < 0.01$. c) Response of diabetic mice to a GTT (3 g/kg) 3 days following injection of empty or NP-encapsulated microgels compared to response of naive mice. d) Area under the curve (AUC) for groups in (c) in addition to GTTs on Day 6 and Day 9 for mice receiving NP-encapsulated microgels on Day 0 and Day 6. Statistical significance was determined by one-way ANOVA with Bonferroni multiple comparison correction (NS: $p > 0.05$). Data represent mean ± standard deviation (a-c) or standard error of the mean (d).

Finally, we evaluated the long-term efficacy of the microgels by monitoring the BG levels of the mice for a total of 4 weeks. On Days 2 and 4 post-administration, the BGs of the microgel-treated group were in the normoglycemic range. On Day 6, the average BG levels of mice receiving microgels increased to over 300 mg/dL (Fig. S10). The BGs of the mice receiving microgels without enzymes were significantly higher, with an average greater than 450 mg/dL (Fig. S10). At this point, both groups were given a second dose of 60 IU/kg insulin (Fig. S11a). Additional GTTs were administered on Day 6 and Day 9 (Fig. S11b), and the responses were similar to that on Day 3, as indicated by the AUCs (Fig. 7d). The mice receiving microgels with enzymes remained cured, with average BGs between 70 and 200 mg/dL for over 2 additional weeks (Fig. 8a). These mice experienced greater glycemic control compared to mice without enzymes (Fig. S12), as evidenced by the significantly reduced area under the BG curve for the first 20 days (Fig. 8b). Therefore, the glucose-sensing enzyme provides both enhanced glucose-responsiveness (Fig. 7b) and enhanced glycemic control (Fig. 8b) in a diabetic mouse model.

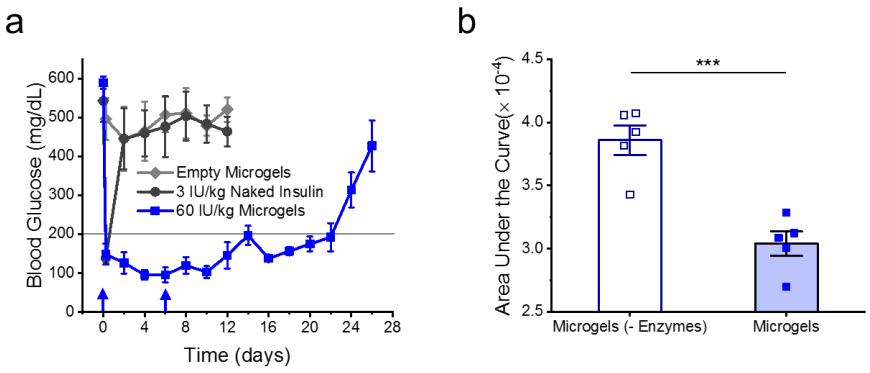

Figure 8. Microgels provide long-term glycemic control in diabetic mice. a) Blood glucose levels of diabetic mice following subcutaneous dosing of 60 IU/kg microgels at days 0 and 6 compared to a single dose of empty microgels or 3 IU/kg naked insulin. b) Area under the curve for the first 20 days of blood glucose levels comparing mice receiving 2 doses of microgels with or without enzymes. Data represent mean ± standard deviation (a) or standard error of the mean (b). Statistical significance was evaluated by a two-tailed, unpaired t-test, and significance is indicated by ***$p < 0.001$.

Discussion

Since patient compliance and adherence to medication regimens is a major challenge in combating diabetes [37-39], reducing dosing frequency through extended release formulations could enhance compliance and therapeutic outcomes [40, 41]. The primary objective of this study was to extend the duration of action of glucose-responsive NPs in diabetic mice, which we accomplished by encapsulating them inside of alginate microgels. A main advantage of this system is that it retains the rapid release kinetics of free NPs in acidic or high glucose conditions with minimal leakage of insulin at physiological pH in vitro (Fig. 2a, S7). Previous studies encapsulating insulin directly in microgels have shown glucose-responsive release through microgel swelling or contracting [42-47]. However, it is difficult to finely control pore size of responsive hydrogels relative to the small size of insulin (< 6 kDa), which may result in either insulin leakage at low glucose concentrations or delayed released at high glucose concentrations. Here, we encapsulate much larger NPs (275 nm) and tune microgel pore size such that NPs remain inside the microgels for extended periods of time while insulin freely diffuses out upon NP degradation. Consistent with literature which reports a reduced permeability of Ba^{2+}-crosslinked microgels [30, 48], we found that changing the crosslinking cation to Ca^{2+} resulted in more rapid release of insulin in acidic conditions (Fig. 2a).

We hypothesize that alginate encapsulation leads to extended, more controlled release of insulin from the NPs due to the creation of a subcutaneous depot in vivo. Using in vivo imaging, we show that microgel-encapsulated NPs are retained at the site of injection longer than free NPs (Fig. 5). Alginate encapsulation likely reduces the diffusivity of the NPs, prevents their premature degradation, and shields them from potential engulfment by immune cell populations. This immunoprotective effect has previously been shown in the context of islet cell transplantation [49, 50]. The greater control over release kinetics is likely independent of the potential fibrotic response to the microgels relative to NPs alone. Using Masson's trichrome staining, we show that the alginate microgels cause minimal inflammation and a very thin fibrous capsule upon subcutaneous implantation for 30 days (Fig. S13). Thus, we anticipate that the enhanced control

of release kinetics results from the preconcentration of NPs in microgels and subsequent depot formation in the subcutaneous space.

As a result of enhanced NP stability, larger doses of NPs can be administered. We previously reported that a dose of 25 IU/kg free NPs has a comparable hypoglycemic effect as 3 IU/kg naked insulin in healthy mice [33]. Here, we show that microgel encapsulation provides significantly reduced risk of hypoglycemia even at 60 IU/kg insulin or 2.4× the maximal dose of free NPs (Fig. 6). In a diabetic mouse model, we show glucose-responsiveness with insulin release occurring within 30 min in response to a glucose challenge (Fig. 7b), which is similar to the response of free NPs [33]. Additionally, we report reproducible responses to glucose tolerance tests on Days 3, 6, and 9 of treatment, similar to the response of naïve mice (Fig. 7d). This enhanced control of insulin release thus enables the potential for much longer durations of normoglycemia with relatively low insulin doses.

We have shown that 2 doses of 60 IU/kg microgels are able to provide glycemic control for a total of 22 days in diabetic animals (Fig. 8). The insulin dose used here (an average of 5.5 IU/kg/day) is consistent with our prior work on free NPs [33]. However, this dose is up to 2 orders of magnitude lower than reported doses for other glucose-responsive delivery systems [19, 24, 51], differences that can partially be attributed to the type of delivery system. Therefore, an additional benefit of this system is the low amount of insulin needed to achieve and sustain normoglycemia.

To further progress this approach, microgels may be fabricated from degradable biomaterials, for example from an oxidized derivative of alginate which hydrolytically degrades [52]. Furthermore, the exogenous enzymes glucose oxidase and catalase may be altered (e.g., through computational design [53], directed evolution [54], or PEGylation [55]) to prevent potential immunogenicity and rapid clearance rates resulting from their repeated administration. Using native alginate and enzymes as models, we show that this strategy may enhance the safety and efficacy of insulin administrations in healthy and diabetic mouse models. The microgels limit the occurrence of hypoglycemia, retain the rapid glucose-responsiveness of the NPs, and maintain glycemic control on the order of weeks. This generalizable strategy of encapsulating glucose-responsive nanoparticles in porous microgels can be adapted for use in other systems to provide long-term, self-regulated insulin delivery.

Acknowledgments

This work was supported in part by project funding provided by the Helmsley Charitable Trust and the Koch Institute Support (core) Grant P30-CA14051 from the National Cancer Institute. L.V. was supported by a NSF Graduate Research Fellowship. We thank the Koch Institute Swanson Biotechnology Center for technical support, specifically the Animal Imaging & Preclinical Testing Core and the High Throughput Screening Core. The authors declare no competing financial interest.

Data Availability

The raw data required to reproduce these findings will be available to download prior to publication. The processed data required to reproduce these findings will be available to download prior to publication.

References

[1] D.R. Owens, B. Zinman, G.B. Bolli, Insulins today and beyond, The Lancet 358(9283) (2001) 739-746. https://doi.org/10.1016/S0140-6736(01)05842-1.

[2] L. Guariguata, D.R. Whiting, I. Hambleton, J. Beagley, U. Linnenkamp, J.E. Shaw, Global estimates of diabetes prevalence for 2013 and projections for 2035, Diabetes Res. Clin. Pract. 103(2) (2014) 137-149. https://doi.org/10.1016/j.diabres.2013.11.002.

[3] K.D. Kochanek, S.L. Murphy, J. Xu, E. Arias, Deaths: Final Data for 2017, Natl. Vital Stat. Rep. (2019).

[4] The Diabetes Control and Complications Trial Research Group, The effect of intensive treatment of diabetes on the development and progression of long-term complications in insulin-dependent diabetes mellitus, N. Engl. J. Med. 1993(329) (1993) 977-986. https://doi.org/l/10.1056/nejm199309303291401.

[5] D.M. Nathan, Long-term complications of diabetes mellitus, New Engl. J. Med. 328(23) (1993) 1676-1685. https://doi.org/l/10.1056/NEJM199306103282306.

[6] D.M. Nathan, DCCT/EDIC Research Group, The diabetes control and complications trial/epidemiology of diabetes interventions and complications study at 30 years: overview, Diabetes Care 37(1) (2014) 9-16. https://doi.org/10.2337/dc13-2112.

[7] N. Jeandidier, S. Boivin, Current status and future prospects of parenteral insulin regimens, strategies and delivery systems for diabetes treatment, Adv. Drug Del. Rev. 35(2) (1999) 179-198. https://doi.org/10.1016/S0169-409X(98)00072-6.

[8] P.E. Cryer, Hypoglycemia, functional brain failure, and brain death, J. Clin. Invest. 117(4) (2007) 868. https://doi.org/10.1172/JCI31669.

[9] C. Cobelli, E. Renard, B. Kovatchev, Artificial pancreas: past, present, future, Diabetes 60(11) (2011) 2672-2682. https://doi.org/10.2337/db11-0654.

[10] B.W. Bequette, Challenges and recent progress in the development of a closed-loop artificial pancreas, Annu. Rev. Control 36(2) (2012) 255-266. https://doi.org/10.1016/j.arcontrol.2012.09.007.

[11] D. DeSalvo, B. Buckingham, Continuous glucose monitoring: current use and future directions, Curr. Diab. Rep. 13(5) (2013) 657-662. https://doi.org/10.1007/s11892-013-0398-4.

[12] U. Klueh, Z. Liu, B. Feldman, T.P. Henning, B. Cho, T. Ouyang, D. Kreutzer, Metabolic biofouling of glucose sensors in vivo: role of tissue microhemorrhages, J. Diabetes Sci. Technol. 5(3) (2011) 583-95. https://doi.org/10.1177/193229681100500313.

[13] D. Rodbard, Continuous glucose monitoring: a review of successes, challenges, and opportunities, Diabetes Technol. Ther. 18(S2) (2016) S2-3-S2-13. https://doi.org/10.1089/dia.2015.0417.

[14] M.A. VandenBerg, M.J. Webber, Biologically inspired and chemically derived methods for glucose-responsive insulin therapy, Adv. Healthcare Mater. 8(12) (2019) 1801466. https://doi.org/10.1002/adhm.201801466.

[15] D. Shen, H. Yu, L. Wang, A. Khan, F. Haq, X. Chen, Q. Huang, L. Teng, Recent progress in design and preparation of glucose-responsive insulin delivery systems, J. Control. Release 321 (2020) 236-258. https://doi.org/10.1016/j.jconrel.2020.02.014.

[16] R. Ma, L. Shi, Phenylboronic acid-based glucose-responsive polymeric nanoparticles: synthesis and applications in drug delivery, Polym. Chem. 5(5) (2014) 1503-1518. https://doi-org.proxy.uchicago.edu/10.1039/C3PY01202F.
[17] A. Matsumoto, T. Kurata, D. Shiino, K. Kataoka, Swelling and shrinking kinetics of totally synthetic, glucose-responsive polymer gel bearing phenylborate derivative as a glucose-sensing moiety, Macromolecules 37(4) (2004) 1502-1510. https://doi.org/10.1021/ma035382i.
[18] A. Matsumoto, M. Tanaka, H. Matsumoto, K. Ochi, Y. Moro-Oka, H. Kuwata, H. Yamada, I. Shirakawa, T. Miyazawa, H. Ishii, Synthetic “smart gel” provides glucose-responsive insulin delivery in diabetic mice, Sci. Adv. 3(11) (2017) eaaq0723. https://doi.org/10.1126/sciadv.aaq0723.
[19] J. Yu, J. Wang, Y. Zhang, G. Chen, W. Mao, Y. Ye, A.R. Kahkoska, J.B. Buse, R. Langer, Z. Gu, Glucose-responsive insulin patch for the regulation of blood glucose in mice and minipigs, Nat. Biomed. Eng. 4 (2020) 499-506. https://doi.org/10.1038/s41551-019-0508-y.
[20] Y. Dong, W. Wang, O. Veiseh, E.A. Appel, K. Xue, M.J. Webber, B.C. Tang, X.-W. Yang, G.C. Weir, R. Langer, Injectable and glucose-responsive hydrogels based on boronic acid–glucose complexation, Langmuir 32(34) (2016) 8743-8747. https://doi.org/10.1021/acs.langmuir.5b04755.
[21] V. Yesilyurt, M.J. Webber, E.A. Appel, C. Godwin, R. Langer, D.G. Anderson, Injectable Self-Healing Glucose-Responsive Hydrogels with pH-Regulated Mechanical Properties, Adv. Mater. 28(1) (2016) 86-91. https://doi.org/10.1002/adma.201502902.
[22] R. Yin, Z. Tong, D. Yang, J. Nie, Glucose-responsive microhydrogels based on methacrylate modified dextran/concanavalin A for insulin delivery, J. Control. Release 152 (2011) e163-e165. https://doi.org/10.1016/j.jconrel.2011.08.064.
[23] K. Podual, F.J. Doyle, N.A. Peppas, Glucose-sensitivity of glucose oxidase-containing cationic copolymer hydrogels having poly (ethylene glycol) grafts, J. Control. Release 67(1) (2000) 9-17. https://doi.org/10.1016/S0168-3659(00)00195-4.
[24] Z. Gu, A.A. Aimetti, Q. Wang, T.T. Dang, Y. Zhang, O. Veiseh, H. Cheng, R.S. Langer, D.G. Anderson, Injectable nano-network for glucose-mediated insulin delivery, ACS Nano 7(5) (2013) 4194-4201. https://doi.org/10.1021/nn400630x.
[25] X. Hu, J. Yu, C. Qian, Y. Lu, A.R. Kahkoska, Z. Xie, X. Jing, J.B. Buse, Z. Gu, H2O2-responsive vesicles integrated with transcutaneous patches for glucose-mediated insulin delivery, ACS Nano 11(1) (2017) 613-620. https://doi.org/10.1021/acsnano.6b06892.
[26] L. Zhao, L. Wang, Y. Zhang, S. Xiao, F. Bi, J. Zhao, G. Gai, J. Ding, Glucose oxidase-based glucose-sensitive drug delivery for diabetes treatment, Polymers 9(7) (2017) 255. https://doi.org/10.3390/polym9070255.
[27] J. Yang, Z. Cao, Glucose-responsive insulin release: Analysis of mechanisms, formulations, and evaluation criteria, J. Control. Release (2017). https://doi.org/10.1016/j.jconrel.2017.01.043.
[28] J. Wang, Z. Wang, J. Yu, A.R. Kahkoska, J.B. Buse, Z. Gu, Glucose-Responsive Insulin and Delivery Systems: Innovation and Translation, Adv. Mater. 32(13) (2020) 1902004. https://doi.org/10.1002/adma.201902004.
[29] K.Y. Lee, D.J. Mooney, Alginate: properties and biomedical applications, Prog. Polym. Sci. 37(1) (2012) 106-126. https://doi.org/10.1016/j.progpolymsci.2011.06.003.
[30] Ý.A. Mørch, I. Donati, B.L. Strand, Effect of Ca2+, Ba2+, and Sr2+ on Alginate Microbeads, Biomacromolecules 7(5) (2006) 1471-1480. https://doi.org/10.1021/bm060010d.
[31] E.M. Bachelder, T.T. Beaudette, K.E. Broaders, J. Dashe, J.M. Fréchet, Acetal-derivatized dextran: an acid-responsive biodegradable material for therapeutic applications, J. Am. Chem. Soc. 130(32) (2008) 10494-10495. https://doi.org/10.1021/ja803947s.

[32] K.E. Broaders, J.A. Cohen, T.T. Beaudette, E.M. Bachelder, J.M. Fréchet, Acetalated dextran is a chemically and biologically tunable material for particulate immunotherapy, Proc. Natl. Acad. Sci. U.S.A. 106(14) (2009) 5497-5502. https://doi.org/10.1073/pnas.0901592106.
[33] L.R. Volpatti, M.A. Matranga, A.B. Cortinas, D. Delcassian, K.B. Daniel, R. Langer, D.G. Anderson, Glucose-Responsive Nanoparticles for Rapid and Extended Self-Regulated Insulin Delivery, ACS Nano 14(1) (2019) 488-497. https://doi.org/10.1021/acsnano.9b06395.
[34] W.C. Johnson Jr, Protein secondary structure and circular dichroism: a practical guide, Proteins. 7(3) (1990) 205-214. https://doi.org/10.1002/prot.340070302.
[35] N.J. Greenfield, Using circular dichroism spectra to estimate protein secondary structure, Nat. Protoc. 1(6) (2006) 2876. https://doi.org/10.1038/nprot.2006.202.
[36] D.N. Brems, P.L. Brown, L.A. Heckenlaible, B.H. Frank, Equilibrium denaturation of insulin and proinsulin, Biochemistry 29(39) (1990) 9289-9293. https://doi.org/10.1021/bi00491a026.
[37] M. Peyrot, A. Barnett, L. Meneghini, P.M. Schumm-Draeger, Insulin adherence behaviours and barriers in the multinational Global Attitudes of Patients and Physicians in Insulin Therapy study, Diabet. Med. 29(5) (2012) 682-689. https://doi.org/10.1111/j.1464-5491.2012.03605.x.
[38] J. Cramer, A. Benedict, N. Muszbek, A. Keskinaslan, Z. Khan, The significance of compliance and persistence in the treatment of diabetes, hypertension and dyslipidaemia: a review, Int. J. Clin. Pract. 62(1) (2008) 76-87. https://doi.org/10.1111/j.1742-1241.2007.01630.x.
[39] R.R. Rubin, Adherence to pharmacologic therapy in patients with type 2 diabetes mellitus, Am. J. Med. 118(5) (2005) 27-34. https://doi.org/10.1016/j.amjmed.2005.04.012.
[40] A.J. Claxton, J. Cramer, C. Pierce, A systematic review of the associations between dose regimens and medication compliance, Clin. Ther. 23(8) (2001) 1296-1310. https://doi.org/10.1016/s0149-2918(01)80109-0.
[41] A. Richter, S.E. Anton, P. Koch, S.L. Dennett, The impact of reducing dose frequency on health outcomes, Clin. Ther. 25(8) (2003) 2307-2335. https://doi.org/10.1016/s0149-2918(03)80222-9.
[42] T. Hoare, R. Pelton, Charge-switching, amphoteric glucose-responsive microgels with physiological swelling activity, Biomacromolecules 9(2) (2008) 733-740. https://doi.org/10.1021/bm701203r.
[43] Z. Gu, T.T. Dang, M. Ma, B.C. Tang, H. Cheng, S. Jiang, Y. Dong, Y. Zhang, D.G. Anderson, Glucose-responsive microgels integrated with enzyme nanocapsules for closed-loop insulin delivery, ACS Nano 7(8) (2013) 6758-6766. https://doi.org/10.1021/nn401617u.
[44] Z. Tang, Y. Guan, Y. Zhang, Contraction-type glucose-sensitive microgel functionalized with a 2-substituted phenylboronic acid ligand, Polym. Chem. 5(5) (2014) 1782-1790. https://doi.org/10.1039/C3PY01190A.
[45] Z. Tang, Y. Guan, Y. Zhang, The synthesis of a contraction-type glucose-sensitive microgel working at physiological temperature guided by a new glucose-sensing mechanism, Polym. Chem. 9(8) (2018) 1012-1021. https://doi.org/10.1039/C8PY00072G.
[46] T. Ye, X. Bai, X. Jiang, Q. Wu, S. Chen, A. Qu, J. Huang, J. Shen, W. Wu, Glucose-responsive microgels based on apo-enzyme recognition, Polym. Chem. 7(16) (2016) 2847-2857. https://doi.org/10.1039/C6PY00179C.
[47] M.Y. Kim, J. Kim, Chitosan microgels embedded with catalase nanozyme-loaded mesocellular silica foam for glucose-responsive drug delivery, ACS Biomater. Sci. Eng. 3(4) (2017) 572-578. https://doi.org/10.1021/acsbiomaterials.6b00716

[48] M.A. Bochenek, O. Veiseh, A.J. Vegas, J.J. McGarrigle, M. Qi, E. Marchese, M. Omami, J.C. Doloff, J. Mendoza-Elias, M. Nourmohammadzadeh, A. Khan, C.-C. Yeh, Y. Xing, D. Isa, S. Ghani, J. Li, C. Landry, A.R. Bader, K. Olejnik, M. Chen, J. Hollister-Lock, Y. Wang, D.L. Greiner, G.C. Weir, B.L. Strand, A.M.A. Rokstad, I. Lacik, R. Langer, D.G. Anderson, J.Oberholzer, Alginate encapsulation as long-term immune protection of allogeneic pancreatic islet cells transplanted into the omental bursa of macaques, Nat. Biomed. Eng. 2(11) (2018) 810-821. https://doi.org/10.1038/s41551-018-0275-1.

[49] E.S. O'Sullivan, A. Vegas, D.G. Anderson, G.C. Weir, Islets transplanted in immunoisolation devices: a review of the progress and the challenges that remain, Endocr. Rev. 32(6) (2011) 827-844. https://doi.org/10.1210/er.2010-0026.

[50] P. de Vos, M.M. Faas, B. Strand, R. Calafiore, Alginate-based microcapsules for immunoisolation of pancreatic islets, Biomaterials 27(32) (2006) 5603-5617. https://doi.org/10.1016/j.biomaterials.2006.07.010.

[51] J. Yu, C. Qian, Y. Zhang, Z. Cui, Y. Zhu, Q. Shen, F.S. Ligler, J.B. Buse, Z. Gu, Hypoxia and H2O2 dual-sensitive vesicles for enhanced glucose-responsive insulin delivery, Nano Lett. 17(2) (2017) 733-739. https://doi.org/10.1021/acs.nanolett.6b03848

[52] K.H. Bouhadir, K.Y. Lee, E. Alsberg, K.L. Damm, K.W. Anderson, D.J. Mooney, Degradation of partially oxidized alginate and its potential application for tissue engineering, Biotechnol. Prog. 17(5) (2001) 945-950. https://doi.org/10.1021/bp010070p.

[53] R.S. Salvat, D. Verma, A.S. Parker, J.R. Kirsch, S.A. Brooks, C. Bailey-Kellogg, K.E. Griswold, Computationally optimized deimmunization libraries yield highly mutated enzymes with low immunogenicity and enhanced activity, Proc. Natl. Acad. Sci. U.S.A. 114(26) (2017) E5085-E5093. https://doi.org/10.1073/pnas.1621233114.

[54] J.R. Cantor, T.H. Yoo, A. Dixit, B.L. Iverson, T.G. Forsthuber, G. Georgiou, Therapeutic enzyme deimmunization by combinatorial T-cell epitope removal using neutral drift, Proc. Natl. Acad. Sci. U.S.A. 108(4) (2011) 1272-1277. https://doi.org/10.1073/pnas.1014739108.

[55] A. Abuchowski, J.R. McCoy, N.C. Palczuk, T. van Es, F.F. Davis, Effect of covalent attachment of polyethylene glycol on immunogenicity and circulating life of bovine liver catalase, J. Biol. Chem. 252(11) (1977) 3582-3586.

Supporting Information

Microgel encapsulated nanoparticles for glucose-responsive insulin delivery

Lisa R. Volpatti, Amanda L. Facklam, Abel B. Cortinas, Yen-Chun Lu, Morgan A. Matranga, Corina MacIsaac, Michael C. Hill, Robert Langer, and Daniel G. Anderson*

Additional Methods

Synthesis of acetalated dextran. Dextran (1 g, MW = 9 – 11 kDa) and pyridinium p-toluenesulfonate (0.0617 mmol) were added to a round-bottom flask and purged with nitrogen. Anhydrous DMSO (10 mL) was subsequently added under nitrogen. After complete dissolution of the dextran, 2- methoxypropene (37 mmol) was added to start the reaction. The reaction was quenched with Et_3N after 10 or 20 min. The product was precipitated and washed with pH 8 water three times and collected by centrifugation (10 min, 8000 rcf; Avanti JXN-26, Beckman Coulter). The product then was lyophilized for two days to yield a white powder.

NMR functionalization analysis. Ac-Dex (5 mg/mL) was hydrolyzed in D_2O containing DCl (10 mM) for 2 h. The samples were analyzed with a 500 MHz 1H NMR (Varian). Cyclic and acyclic acetal content was measured by quantifying the amount of acetone and methanol produced by the hydrolysis of Ac-Dex and normalizing by the protons on the anameric carbon of the glucose ring.

Dynamic light scattering. Lyophilized nanoparticles were suspended in ultrapure water and filtered through 0.8 µm membrane filters to yield a concentration ~ 0.5 mg/mL before characterization by dynamic light scattering (DLS; Zetasizer Nano ZS, Malvern Instruments).

Protein loading. The loading capacities of insulin and GOx in nanoparticles without catalase were calculated using Eq. (1), and the loading efficiencies were calculated from Eq. (2).

$$\text{loading capacity} = \frac{\text{mass of encapsulated protein}}{\text{total mass of NP}} \times 100 \quad (1)$$

$$\text{loading efficiency} = \frac{\text{mass of encapsulated protein}}{\text{starting mass of protein}} \times 100 \quad (2)$$

Protein content was measured after degrading a known mass of nanoparticles in 1 M acetic acid. Insulin was quantified by high performance liquid chromatography (Agilent 1100 Series) with an Atlantis® T3 column (5 µm, Waters). GOx was quantified by enzymatic activity using an Amplex® Red Glucose/Glucose Oxidase Assay Kit (Life Technologies).

Perifusion insulin release. To determine insulin release under flow conditions, microgels were inserted into a perifusion system chamber (Biorep). Acetate buffer was pumped through the chambers at a rate of 10 µL/min, collected into a 96-well plate every 15 min, and analyzed for protein content.

Supplemental Figures

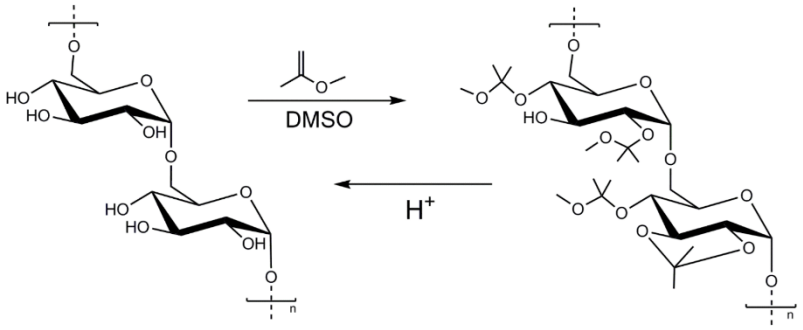

Figure S1. Schematic of acetalated-dextran (Ac-dex) synthesis.

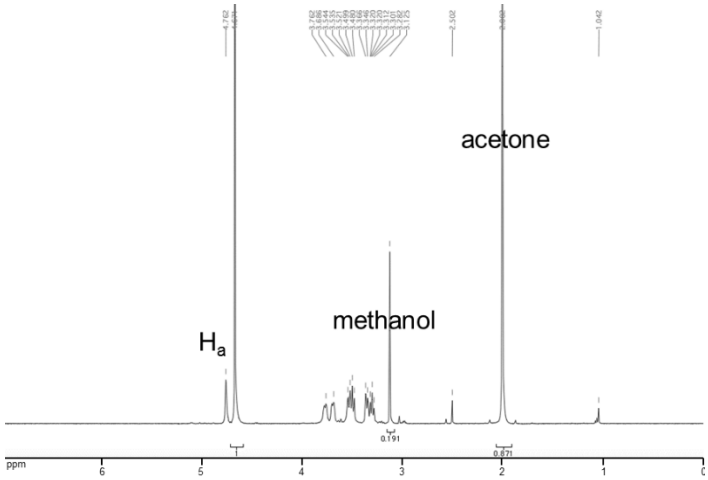

Figure S2. Example ^{1}H NMR spectrum of Ac-dex upon incubation in deuterium chloride showing the methanol and acetone peaks used to analyze the polymer modification percentage. A 10 min reaction time yields dextran with 55% cyclic acetal modifications, and a 20 min reaction time yields dextran with 71% cyclic acetal modifications.

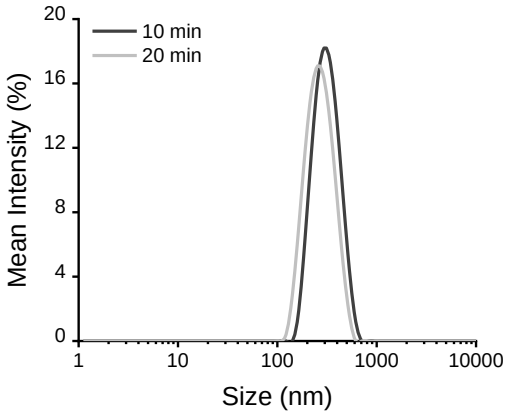

Figure S3. Dynamic light scattering of nanoparticles synthesized from Ac-dex that had been reacted for 10 or 20 min.

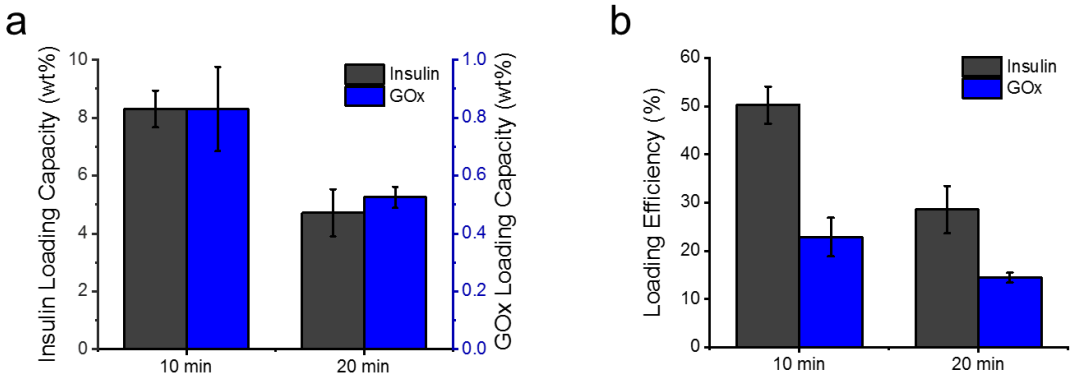

Figure S4. Protein loading. a) Loading capacities and b) loading efficiencies of insulin and glucose oxidase as defined in the supplementary experimental section.

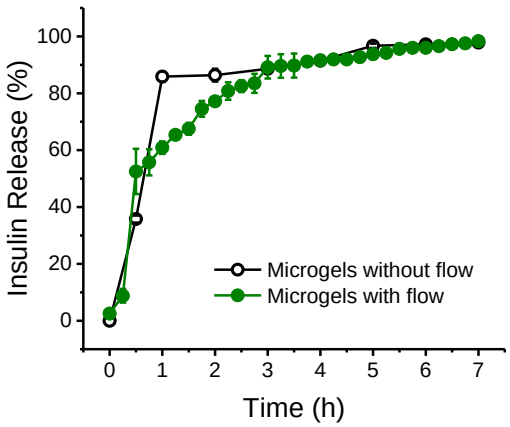

Figure S5. Acid-mediated insulin release from nanoparticle-encapsulated microgels incubated in a centrifuge tube with acetate buffer at 37 °C with agitation (black open circles) compared to microgels in a perifusion system chamber (37 °C) subjected to a flow rate of 10 µL/min acetate buffer (green solid circles).

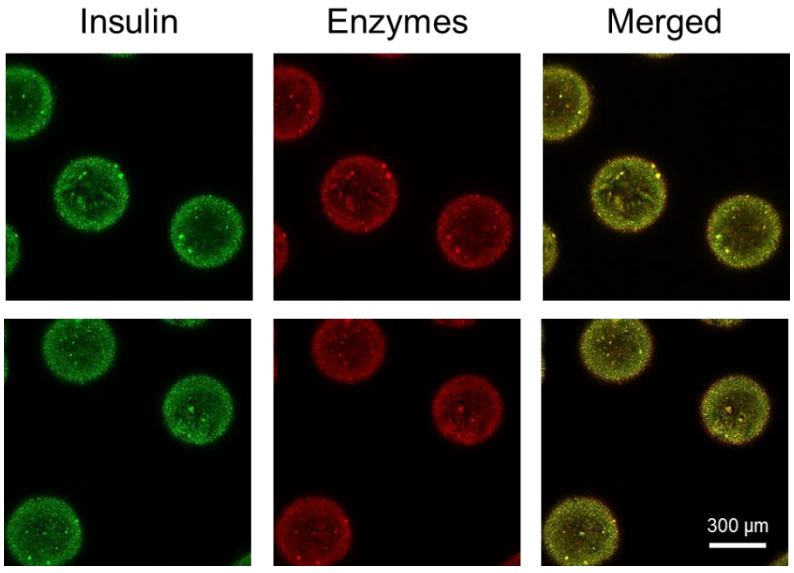

Figure S6. Additional confocal microscopy images (at a given z plane) of microgels containing nanoparticles encapsulated with FITC-insulin and AF647-glucose oxidase. Due to the opacity of the nanoparticles, limited light can pass through the center of the microgels.

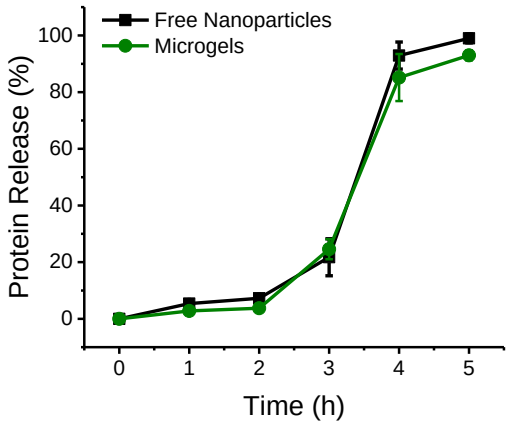

Figure S7. Comparison of glucose-mediated insulin release from NPs and microgels. NPs (2 mg) or microgels (100 µL) were incubated in a total of 200 µL PBS with 400 mg/dL glucose. Every hour, the nanoparticles were centrifuged, 50 µL supernatant was removed for protein analysis, and 50 µL fresh buffer was added to the samples.

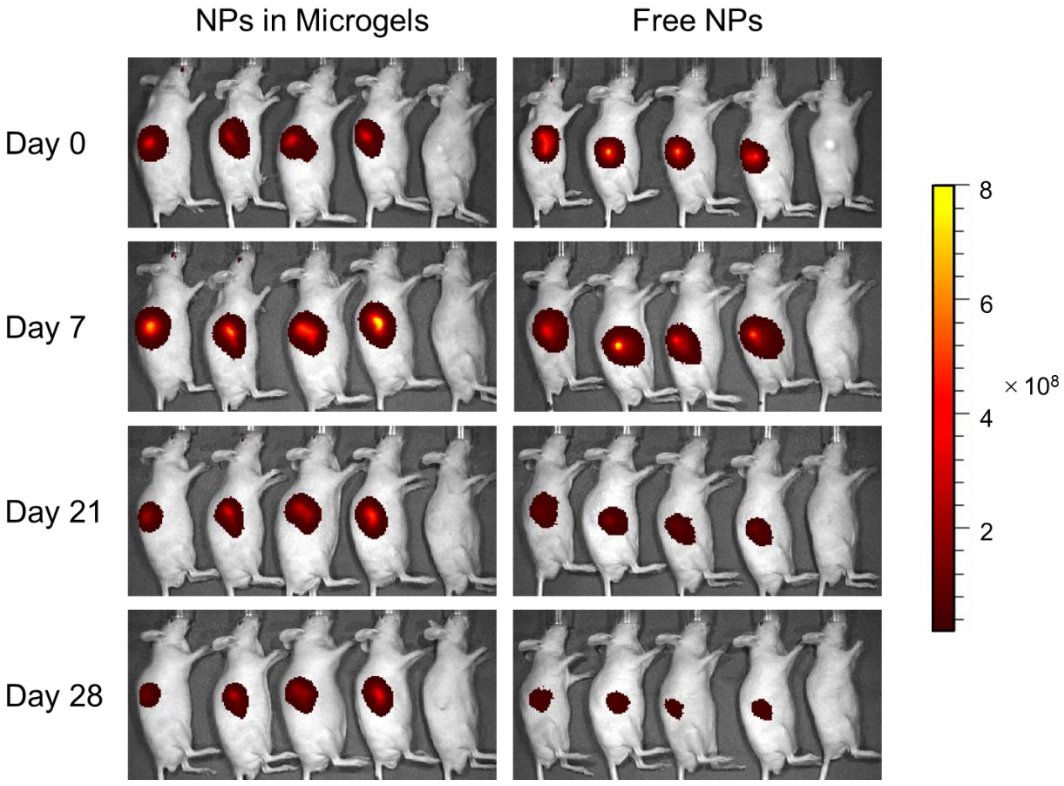

Figure S8. In vivo fluorescent images of NP-encapsulated microgels or free NPs containing AF680-dextran (10 kDa) subcutaneously injected in healthy, hairless mice at a dose equivalent to 60 IU/kg insulin. N = 4 mice per group, with the fifth mouse in each group receiving empty microgels or empty nanoparticles as a control.

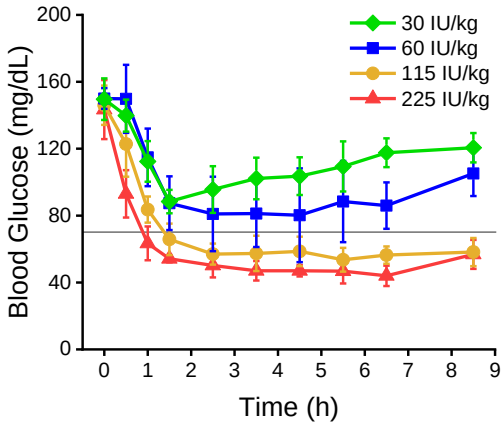

Figure S9. BG levels of healthy mice receiving microgels at insulin doses of 30, 60, 115, and 225 IU/kg. Data represent mean ± standard deviation.

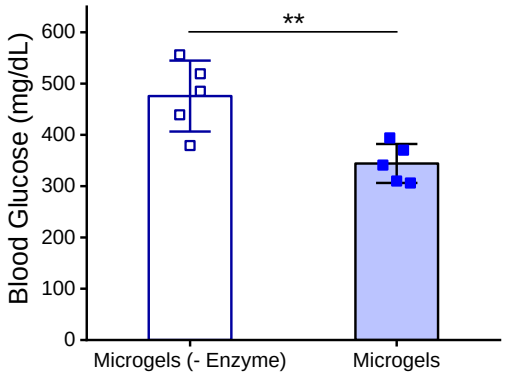

Figure S10. BG levels of diabetic mice 6 days after receiving a dose of 60 IU/kg microgels with or without enzymes, prior to administration of a second dose. Data represent mean ± standard deviation. Statistical significance is indicated by **p < 0.01.

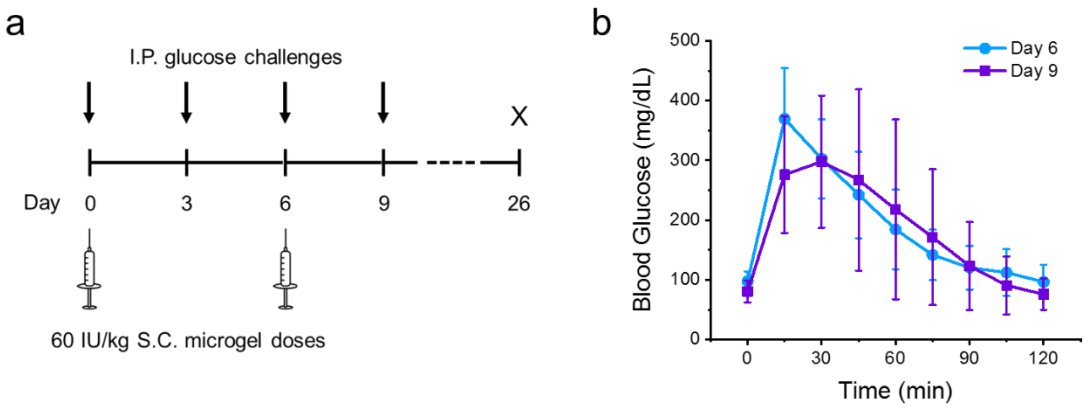

Figure S11. Experimental timeline and glucose response. a) Microgels were dosed subcutaneously on days 0 and 6, and mice were administered intraperitoneal glucose tolerance tests on days 0, 3, 6, and 9. b) Response to glucose tolerance tests (3 g/kg) on days 6 and 9. Data represent mean ± standard deviation.

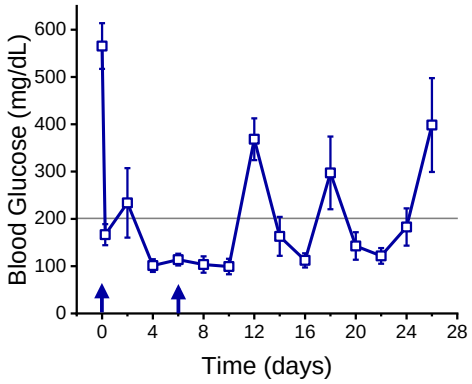

Figure S12. BG levels of diabetic mice following subcutaneous dosing of 60 IU/kg microgels without enzymes at days 0 and 6. Data represent mean ± standard deviation.

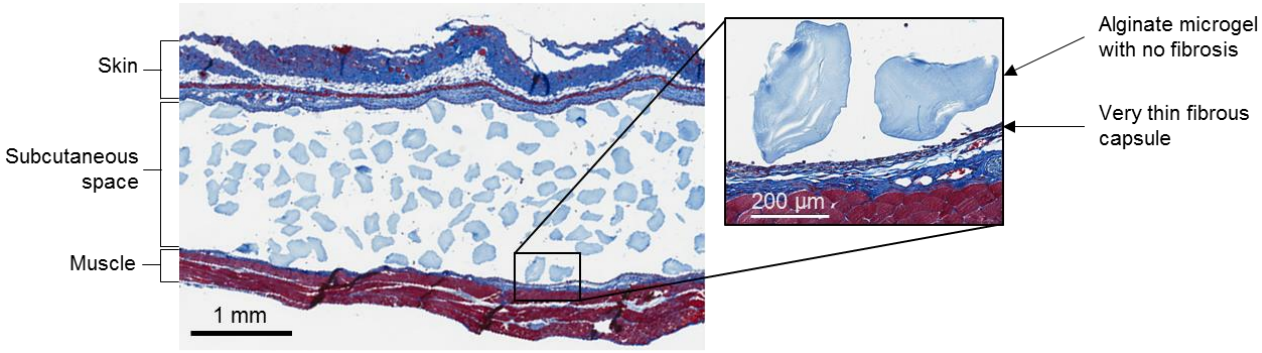

Figure S13. Representative Masson's trichrome staining of mouse subcutaneous tissue containing alginate microgels 30 days post-injection.